Journal of Organometallic Chemistry, 268 (1984) 275–293
Elsevier Sequoia S.A., Lausanne – Printed in The Netherlands

MOLECULAR ORBITAL ANALYSIS OF THE BONDING IN HIGH NUCLEARITY GOLD CLUSTER COMPOUNDS

KEVIN P. HALL, DAVID I. GILMOUR and D. MICHAEL P. MINGOS*
Inorganic Chemistry Laboratory University of Oxford, South Parks Road, Oxford OX1 3QR (Great Britain)
(Received February 8th, 1984)

Summary

Extended Hückel molecular orbital calculations on high nuclearity gold clusters of the general type $[Au(AuPH_3)_n]^{x+}$ have demonstrated that they can be classified into two broad topological classes according to the three-dimensional disposition of the peripheral gold atoms. If they lie approximately on a sphere they are characterised by a total of $12n + 18$ valence electrons, but if they adopt a toroidal or eliptical arrangement the total electron count is $12n + 16$. The computed energy differences between alternative polyhedral geometries is generally small and accounts for the stereochemical non-rigidity of the gold cluster compounds in solution. Detailed aspects of the structures of the high nuclearity gold cluster compounds have been interpreted in terms of molecular orbital calculations on clusters derived from the centred chair $[Au_7(PH_3)_6]^+$ by edge- and face-capping with $Au(PH_3)^+$ fragments.

In 1976 we reported a theoretical analysis of the bonding in high nuclearity gold tertiary phosphine cations [1] which correctly predicted the stoicheiometry and structure of the first example of an icosahedral metal cluster compound, viz. $[Au_{13}Cl_2(PMe_2Ph)_{10}](PF_6)_3$ [2,3]. Since that time several groups have been actively involved in the synthesis of new gold cluster compounds and the study of their structures in the solid and solution states has revealed a complexity exceeding that observed for other Group B metals [4–6]. It is the aim of this paper to interpret these structural complexities in terms of a simple bonding model derived from semi-empirical molecular orbital calculations. This analysis draws heavily on the *isolobal* qualities of the $AuPR_3$ fragment developed for low nuclearity clusters in a previous publication [7].

Recently, we have suggested that the solid state structures of high nuclearity gold cluster compounds may be rationalised in terms of the scheme illustrated in Fig. 1. The structures of all the known compounds can be derived from the centred crown $[Au_9(PR_3)_8]^{3+}$ and centred chair $[Au_7(PR_3)_6]^+$ moieties illustrated at the top of the Figure [8]. The former has been found for example in $[Au_9\{P(p$-

0022-328X/84/$03.00

$C_6H_4OMe)_3\}_8]^{3+}$ (II) [9], and the latter although not observed as an independent moiety is the building block for the numerous higher nuclearity gold cluster cations illustrated in the Figure [9–14]. The clusters shown at the left hand side of Fig. 1 are characterised by a total of $12n + 16$ electrons and are derived from I by adding AuL fragments to three atom sequences on the peripherary of the cluster. In contrast, the clusters on the right hand side of Fig. 1 are derived from I by the addition of either AuL or Au_3L_3 triangular fragments along the three-fold axis and are characterised by a total of $12n + 18$ electrons. This electronic and structural difference can be interpreted in terms of the molecular orbital characteristics of the parent moieties I

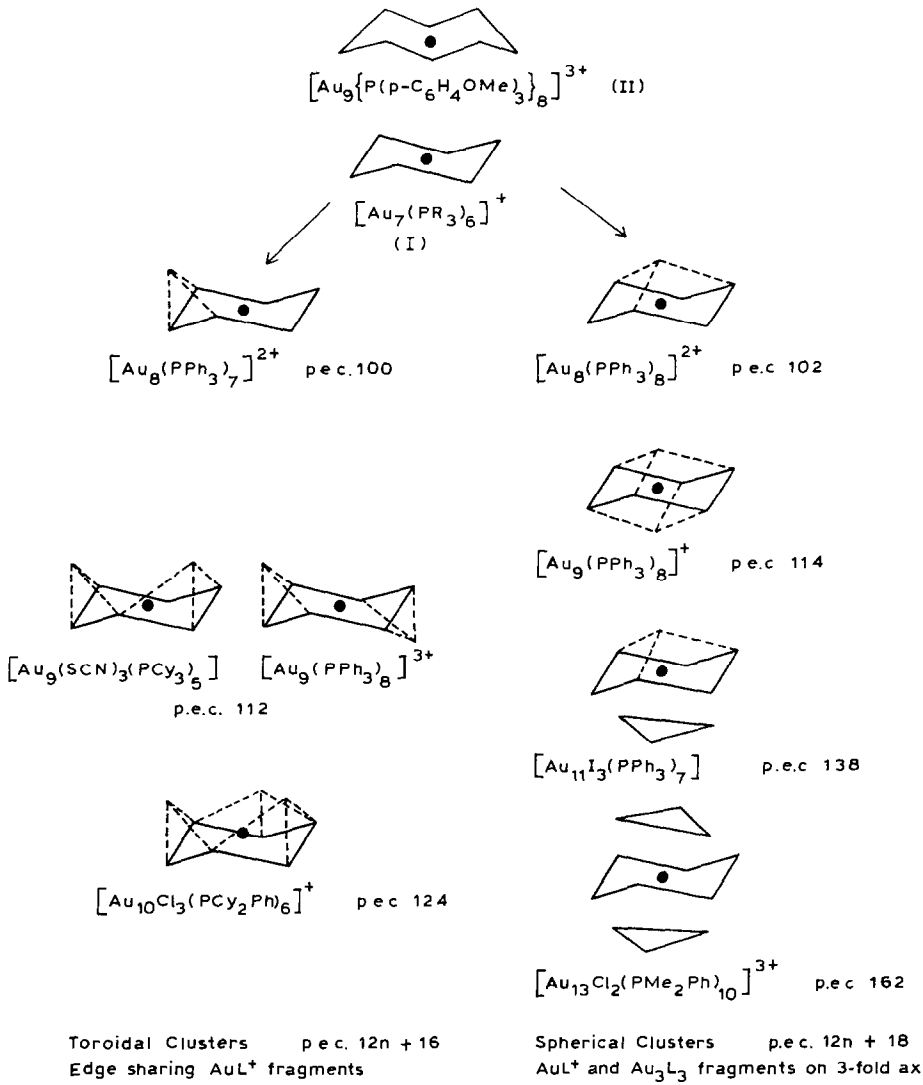

Fig. 1. Summary of structural features of gold cluster cations. On the left hand side toroidal clusters with $12n + 16$ valence electrons can be derived from $[Au_7(PR_3)_6]^+$ (centred chair) by edge-bridging with $AuPR_3^+$ fragments. On the right hand side spherical clusters with $12n + 18$ electrons are generated by the addition of $AuPR_3^+$ or $Au_3P_3^+$ fragments along the three-fold axis.

and II and this analysis forms the major part of this paper. However, prior to this analysis it is worth emphasising that the observed solid state structures summarised in Fig. 1 represent rather shallow minima on a very soft potential energy surface. This conclusion has been supported by solution NMR studies which have indicated that the gold clusters are stereochemically non-rigid in solution, and the observation that these gold cluster compounds can exhibit skeletal isomerism, i.e. a given compound crystallises in more than one crystalline modification with alternative skeletal geometries [15]. Given these observations it would appear to be over optimistic to attempt to give a detailed explanation of the observed solid state structures and a more appropriate starting point might be derived from the topological distinction between the two classes of gold cluster compound illustrated in Fig. 1. The peripheral gold atoms on the right hand side of Fig. 1 lie approximately on the surface of a sphere, whereas those on the left hand side define a torus or elipsoid. This topological distinction provides a rather neat explanation for the $12n + 18$ and $12n + 16$ electron counting rules which are relevant for this class of cluster compound. Therefore, this paper is divided into two parts: the first provides a general analysis of the $12n + 16$ and $12n + 18$ electron counting rules and is based on the spherical harmonic mode of analysis developed for clusters by Stone [16,17]; the second gives a detailed analysis of the bonding in the compounds illustrated in Fig. 1 derived from extended Hückel molecular orbital calculations and which provides a more detailed interpretation of the bond lengths observed in the solid state. The basic features of the mode of calculation have been described previously [18] and the parameters used in the calculations are described in the Appendix.

General bonding model for spherical and toroidal clusters

For a bare gold cluster, Au_n^{x+}, with the gold atoms lying approximately on a sphere the bonding interactions are dominated by the overlap of gold $6s$ orbitals, since the large $6s$–$6p$ promotion energy discourages an effective contribution from the $6p$ orbitals [1]. In the phosphine cluster cations, $[AuPR_3]_n^{x+}$, the bonding is also dominated by the $6s$ orbitals, although significant admixtures of $5d_{z^2}$ and $6p_z$ character are introduced as a result of the coordination of the PR_3 ligands [1]. If attention is focussed on the topology of the cluster rather than the precise location of the gold atoms in space then the most flexible bonding model is that which is independent of the spherical coordinates of the gold atoms. Such a model has been developed for borane and metal clusters by Stone [16,17]. If the angular positions of the gold atoms are defined by the general coordinates θ_i and ϕ_i $(i = 1 - n)$ the molecular orbital coefficients can be derived from spherical harmonics according to the following equation:

$$\Psi_{lm} = \sum_i Y_{lm}(\theta_i, \phi_i)\sigma_i$$

where σ_i are the relevant gold $6s$ wave functions. The cluster molecular orbitals can therefore be classified according to their azimuthal and magnetic quantum numbers l and m, i.e. as S^o $(l = 0,\ m = 0)$; P^o $(l = 1,\ m = 0,\ \pm 1)$; D^o $(l = 2,\ m = 0,\ \pm 1\ \pm 2)$ etc. In common with atomic orbitals which are also expressed in terms of spherical harmonic functions, these cluster molecular orbitals are characterised by the number of nodal planes which they possess. Furthermore, because of the significant $6s$–$6s$

overlap integrals between adjacent gold atoms the number of nodal planes accurately reflects the relative energies of the molecular orbitals. Indeed when $12 \geqslant n > 6$ then only the S^{σ} and P^{σ} functions which are illustrated below are bonding.

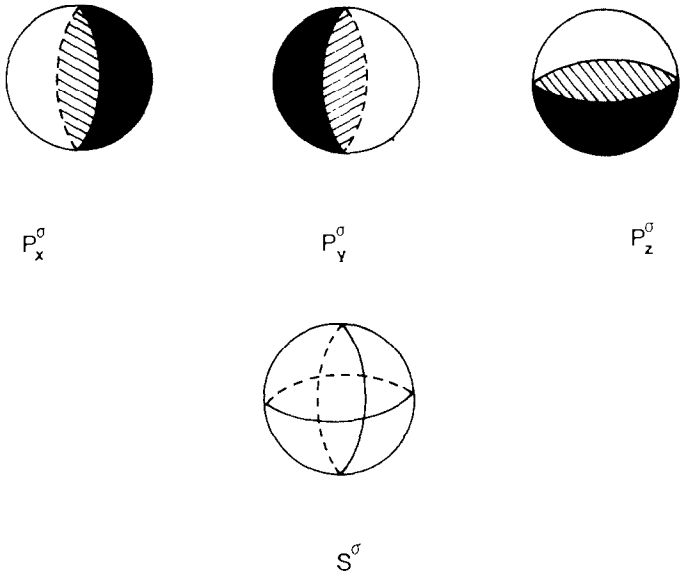

It follows that for all spherical clusters of the type Au_n ($12 \geqslant n > 6$) are characterised by a total of only four bonding skeletal molecular orbitals.

Figure 2 illustrates the orbitals of an icosahedral Au_{12} cluster and underlines the relationship between nodal characteristics and orbital energies. Clearly only the S^{σ} and P^{σ} functions are bonding. This bonding pattern is reinforced by the presence of a central gold atom which has $6s$ and $6p$ valence orbitals which overlap effectively with the bonding S^{σ} and P^{σ} skeletal molecular orbitals illustrated in Fig. 2. The resultant molecular orbitals are more localised on the central gold atom than the peripheral gold atoms. The phosphine ligands accentuate the radial gold–gold bonding interactions by suitably rehybridising the gold $5d_{z^2}$, $6s$ and $6p_z$ orbitals of the peripheral gold atoms. The occurrence of strong radial gold–gold bonding compared with the tangential gold–gold bonding is supported by the fact that the radial gold–gold bond lengths are consistently shorter [1, 3, 4]. Furthermore, it is consistent with the observed stereochemical non-rigidity of these cluster compounds [3,4].

Table 1 summarises the computed sum of one electron energies for some spherical nine and thirteen atom "bare" and molecular gold cluster species. It is apparent that the terminal ligands make little difference to the relative energies of the alternative polyhedral geometries. It is interesting that the computed energy differences are relatively small, i.e. 0.32 for Au_9^{3+} and 0.60 eV for Au_{13}^{5+}. The radial Au–Au bonding interactions are rather insensitive to the polyhedral geometries chosen and the calculated energies given in Table 1 reflect differences in the weaker tangential Au–Au interactions. Since the tangential Au–Au interactions are greatest for polyhedra with the maximum number of edges, the calculations show a slight preference for deltahedra.

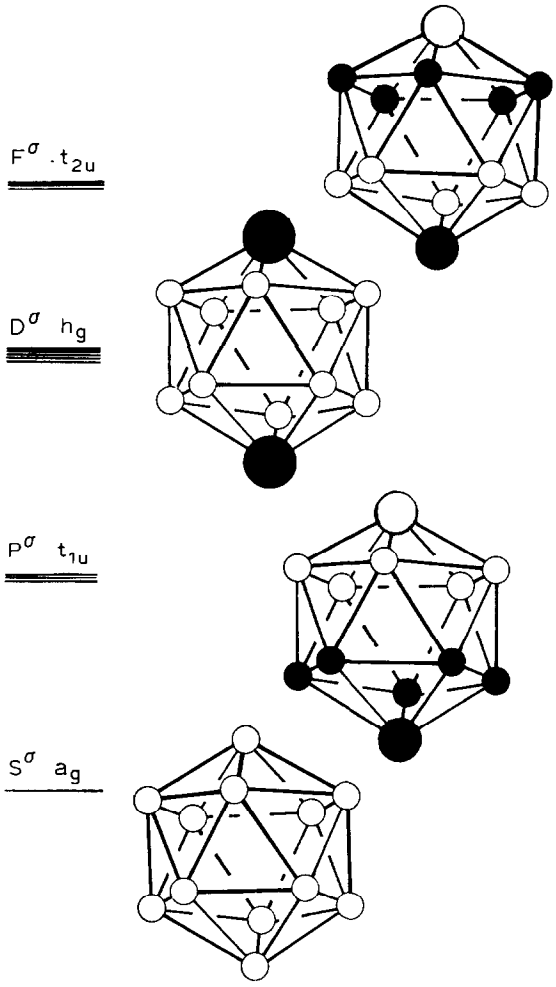

Fig. 2. The skeletal molecular orbitals for an icosahedral Au_{12} cluster derived from the overlap of gold 6*s* orbitals.

The $12n + 18$ electron rule for spherical gold cluster compounds $[Au(AuPR_3)_n]^{x+}$ is a direct consequence of the formation of four (S^{σ} and P_x^{σ}, P_y^{σ} and P_z^{σ}) skeletal molecular orbitals (i.e. 8 electrons occupy these orbitals, $10(n + 1)$ electrons occupy the 5*d* shells and $2n$ the Au–P bonding molecular orbitals giving a total of $12n + 18$). Figure 1 gives some specific examples of gold cluster compounds with spherical topologies and which conform to the $12n + 18$ electron rule.

In contrast the toroidal clusters in Fig. 1 are characterised by a total of $12n + 16$ electrons. This difference can be traced to a removal of the degeneracy associated with the P_x^{σ}, P_y^{σ} and P_z^{σ} skeletal molecular orbitals when the symmetry is reduced from spherical to eliptical ($D_{\infty h}$). In an eliptical or toroidal cluster the P_x^{σ} and P_y^{σ} functions retain their bonding character, but the P_z^{σ} function becomes either non-bonding or antibonding. The reason for this can most easily be appreciated by

TABLE 1

SUM OF COMPUTED ONE-ELECTRON ENERGIES FOR SOME SPHERICAL Au_9 AND Au_{13} CLUSTERS (eV)

Geometry	Au_9^{3+}	$[Au_9L_8]^{3+}$
Cubic	−1132.4	−1313.8
Square-antiprismatic	−1132.2	−1313.7
dodecahedral	−1132.5	−1314.0
	Au_{13}^{5+}	$[Au_{13}L_{12}]^{5+}$
icosahedral	−1631.9	−1903.6
cuboctahedral	−1631.1	−1903.0
anti-cuboctahedral	−1631.1	−1903.0

reference to the illustration below:

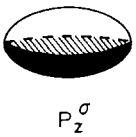

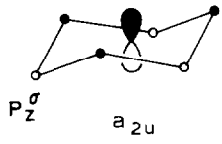

For toroidal gold cluster compounds, adjacent gold atoms lie above and below the nodal plane of the P_z^σ function and consequently the interactions between these atoms is antibonding. This antibonding character can be mitigated somewhat if pairs of adjacent atoms are located on the same side of the plane, e.g. in $[Au_9(PPh_3)_8]^{3+}$ in Fig. 1 but cannot be lost completely. It follows that if these toroidal clusters are characterised by only three bonding skeletal molecular orbitals then the total electron count is $12n + 16$. Specific examples of toroidal gold cluster compounds are illustrated in Fig. 1.

Calculations on $[Au_9(PH_3)_8]^{3+}$ with the alternative geometries shown in Fig. 1 established that their calculated energies differ by less than 0.3 eV. Therefore, it is hardly surprising that these compounds are stereochemically non-rigid and exhibit skeletal isomerism in the solid state [3–5,9,15].

It has been common in cluster chemistry to associate electron addition with the opening-out of the polyhedral cage [19]. For example, in borane and metal carbonyl cluster chemistry the following transformations are commonplace:

$$\textit{Closo-} \xrightarrow{2e^-} \textit{Nido-} \xrightarrow{2e^-} \textit{Arachno-}$$

However, the molecular orbital analysis described above suggests that the addition of an electron pair to a *toroidal* ($12n + 16$) cluster should result in a more compact *spherical* ($12n + 18$) cluster. Such a transformation has been achieved electrochemically for $[Au_9(PPh_3)_8]^{3+}$ and is illustrated below [20]:

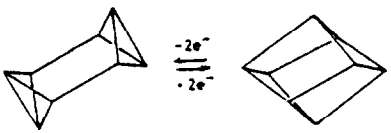

Detailed analysis of toroidal clusters

Figure 3 illustrates the skeletal molecular orbitals for $[Au_7(PH_3)_6]^+$, with a centred chair geometry, because this fragment appears to be a very important structural component in gold cluster chemistry (see Fig. 1). This toroidal cluster is characterised by three bonding skeletal molecular orbitals, which have the nodal characteristics common to the S^σ, P_x^σ and P_y^σ functions derived for the general eliptical situation in the previous section. These molecular orbital wave functions are concentrated primarily on the central atom.

A comparison of the computed overlap populations for $[Au_7(PH_3)_6]^+$ and $[Au_9(PH_3)_8]^{3+}$, with a centred crown geometry, has indicated two important general features. Firstly, the radial overlap populations are larger than the peripheral overlap populations and secondly the latter diminish as the size of the ring is increased. Since the number of bonding skeletal molecular orbitals remains constant then as the ring size is increased the bonding electron density is less localised in specific bonds.

As noted in the introduction the skeletal geometries of $[Au_8(PPh_3)_7]^{2+}$, $[Au_9(PPh_3)_8]^{3+}$, $[Au_9(SCN)_3(PCy_3)_5]$ and $[Au_{10}Cl_3(PCy_2Ph)_6]^+$ can be derived from the centred chair geometry of $[Au_7(PR_3)_6]^+$ by the addition of $AuPR_3^+$ fragments to three atom sequences of the peripheral atoms. The effect of these interactions on the skeletal molecular orbitals of $[Au_7(PR_3)_6]^+$ is illustrated in Fig. 3. The primary effect is the stabilisation of the S^σ, P_x^σ and P_y^σ skeletal molecular orbitals and the retention of P_z^σ as an antibonding orbital. The latter is necessary because the stabilisation of the latter to a sufficient extent to permit electron occupation would result in a change in cluster topology from toroidal to spherical.

$[Au_8(PPh_3)_7]^{2+}$ can be modelled by placing an $AuPH_3$ fragment above a three atom sequence of gold atoms of the $[Au_7(PH_3)_6]$ chair as shown below:

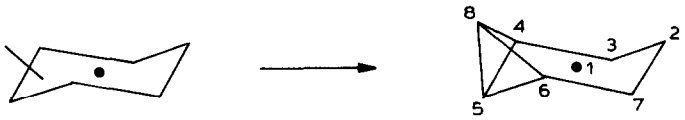

The $1a'(S^\sigma)$ orbital is stabilised to a slight extent by an in-phase interaction with the $6s$ orbital of the additional $AuPH_3$ fragment. The degeneracy of the e_u set of $Au_7(PH_3)_6$ is removed. The energy of the $1a''(P_y^\sigma)$ component remains essentially unaltered as there are no orbitals of suitable symmetry and energy on the additional $AuPH_3$ fragment with which it can interact. The $2a'(P_x^\sigma)$ component is stabilised by an in-phase interaction with the $6p_x$ orbital of the central gold atom and an sp_x hybrid orbital on Au(5), as illustrated in Fig. 3. The energy of the $3a'(P_z^\sigma)$ orbital is stabilised somewhat by the introduction of the extra $AuPH_3$ fragment but not sufficiently to make its energy comparable to that of $1a''(P_y^\sigma)$ and $2a'(P_x^\sigma)$. A charge of $+2$ would be predicted for this cluster compound, corresponding to the occupation of the levels $1a'(S^\sigma)$, $2a'(P_x^\sigma)$ and $1a''(P_y^\sigma)$.

The gold–gold bond lengths found from an X-ray crystallographic study of $[Au_8(PPh_3)_7][NO_3]_2$ [11] are accounted for nicely by the computed overlap populations for $[Au_8(PH_3)_7]^{2+}$ and are summarised in Table 2.

The computed overlap populations and bond lengths reflect the nodal characteris-

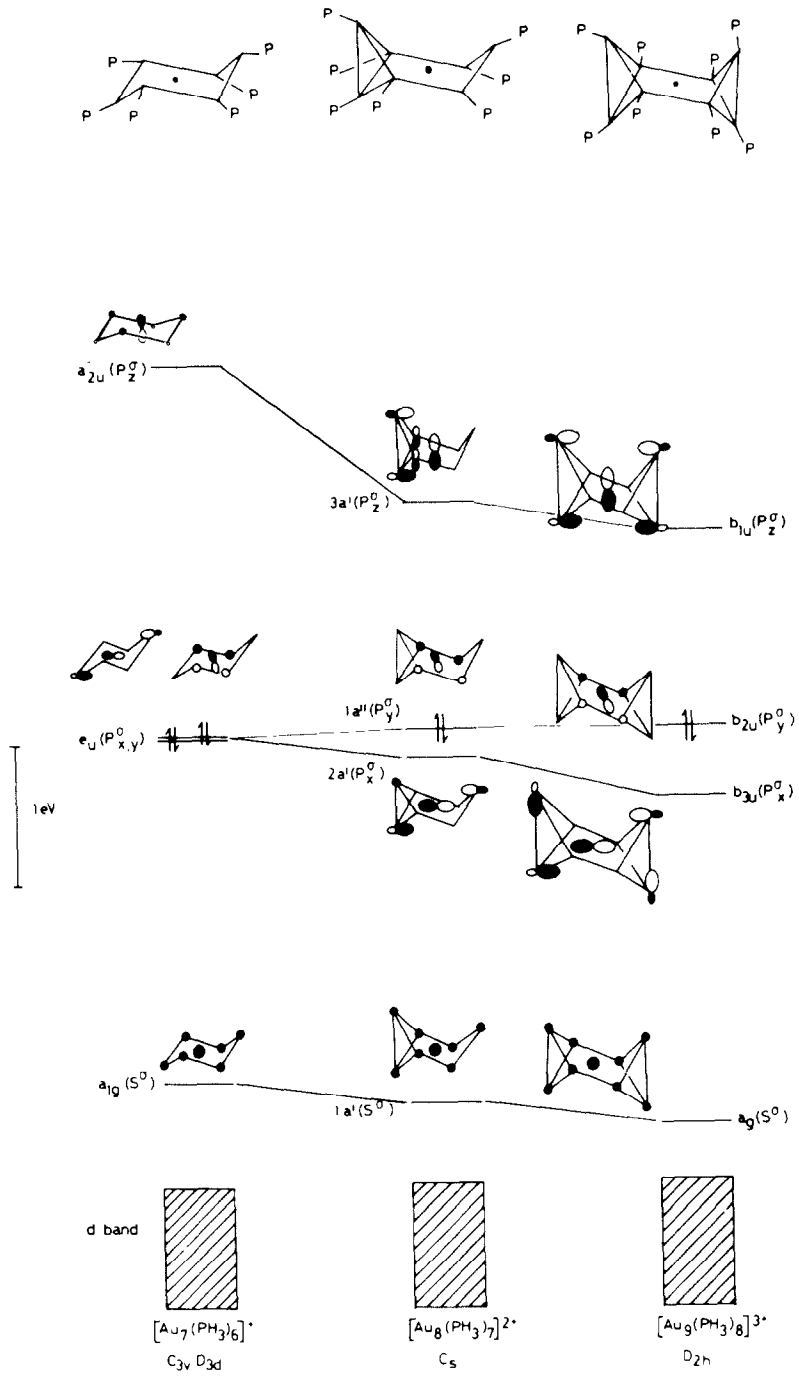

Fig. 3. The skeletal molecular orbitals for Au_7, Au_8 and Au_9 toroidal clusters are illustrated.

TABLE 2

Au–Au BOND LENGTHS FOUND IN $[Au_8(PPh_3)_7][NO_3]_2$ AND COMPUTED OVERLAP POPULATIONS FOR $[Au_8(PH_3)_7]^{2+}$

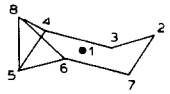

Bond	Bond length (Å)	Computed overlap population
1–7	2.672(5)	0.25
1–3	2.663(5)	0.25
1–2	2.629(6)	0.24
1–4	2.688(6)	0.21
1–6	2.673(5)	0.21
1–8	2.720(3)	0.17
1–5	2.724(6)	0.15
2–3	2.842(5)	0.14
2–7	2.829(5)	0.14
6–7	2.817(5)	0.14
3–4	2.796(5)	0.14
5–8	2.706(5)	0.12
5–6	2.942(5)	0.10
4–5	2.901(5)	0.10
4–8	2.879(5)	0.09
6–8	2.923(6)	0.09

tics of the higher lying molecular orbitals. The atomic orbitals of the additional gold atom Au(8) make little contribution to the HOMO ($1a''$, P_y^σ) but have a bonding interaction with the central gold atom, Au(1), and Au(5). Hence the bonding of Au(8) is essentially a 3-centre interaction between the capping gold atom, and Au(1) and Au(5). This interaction is reflected in the bond lengths given in Table 2.

By capping the opposite three atom sequence with another $AuPH_3$ fragment (see below), a cluster of stoicheiometry $Au_9(PH_3)_8$ having D_{2h} symmetry is generated:

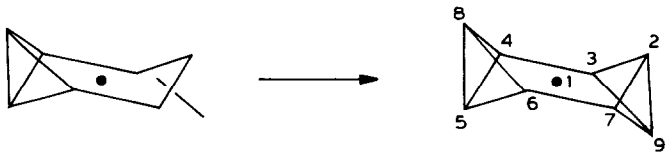

The effects of this edge-bridging on the molecular orbitals are similar to those noted in the previous example. The $a_g(S^\sigma)$ orbital is stabilised slightly by the extra in-phase overlap of the orbitals of the additional gold atom, Au(9). The HOMO remains unchanged in energy as there are no orbitals of suitable symmetry and energy to interact with the $b_{2u}(P_y^\sigma)$ orbital. However, the $b_{3u}(P_x^\sigma)$ orbital is stabilised by 0.3 eV by the in-phase interaction of an sp_x hybrid of the additional $AuPH_3$ fragment and the $2a'$ orbital of $[Au_8(PH_3)_7]^{2+}$. The $b_{1u}(P_z^\sigma)$ orbital remains high lying and unoccupied but is stabilised slightly with respect to the $3a'$ orbital.

The geometry discussed above has been observed in the cluster compound $[Au_9\{P(p\text{-}C_6H_4Me)_3\}_8][PF_6]_3$ [12]. The nodal characteristics of the $a_g(S^\sigma)$, $b_{3u}(P_x^\sigma)$ and $b_{2u}(P_y^\sigma)$ orbitals are reflected in the computed overlap populations and in the observed bond lengths which are given in Table 3. For example, the atomic orbitals

TABLE 3

Au–Au BOND LENGTHS FOUND IN $[Au_9\{P(p\text{-}C_6H_4Me)_3\}_8][PF_6]_3$ AND COMPUTED OVERLAP POPULATIONS FOR $[Au_9(PH_3)_8]^{3+}$

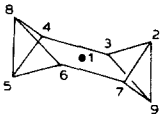

Bond	Bond length (Å)	Computed overlap population
1–3, 1–4, 1–6, 1–7	2.689(3)	0.21
1–2, 1–5, 1–8, 1–9	2.729(3)	0.16
2–9, 5–8	2.752(3)	0.11
3–4, 6–7	2.790	0.14
all others	2.87 ± 0.02	0.10

of the additional gold atom Au(9) have little interaction with the HOMO but have a significant bonding interaction with the $2a'(P_x^a)$ orbital of $[Au_8(PH_3)_7]^{2+}$. Hence the bond lengths between Au(9) and, Au(1) and Au(2) are expected to be shorter than those between Au(9) and Au(3) and Au(7). This pattern is reflected in the observed bond lengths. The radial bonds have consistently larger overlap populations and shorter bond lengths than the peripheral bonds.

The compounds $[Au_8(PPh_3)_7]^{2+}$, $[Au_9(SCN)_3(PCy_3)_5]$ and $[Au_{10}Cl_3(PCy_2Ph)_6][NO_3]$ are all structurally closely related, as seen from Fig. 1. The addition of the bridging $AuPH_3$ fragments in these compounds is associated with a displacement of the central gold atom along the three-fold axis and towards the bridging groups. Calculations on $[Au_8(PPh_3)_7]^{2+}$ with the central gold atom displaced 0.8 Å in this fashion demonstrated that the energies of the individual molecular orbitals were little affected by this distortion.

The structures are related to a centred chair of gold atoms by bridging 2 edges at a time with a gold atom; once for $[Au_8(PH_3)_7]^{2+}$; twice for $[Au_9(PH_3)_8]^{3+}$ (which is used to model $[Au_9(SCN)_3(PCy_3)_5]$ and three times for $[Au_{10}(PH_3)_9]^{4+}$ (which is used to model $[Au_{10}Cl_3(PCy_2Ph)_6]^+$).

$[Au_8(PPh_3)_7]^{2+}$

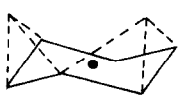

$[Au_9(SCN)_3(PCy_3)_5]$

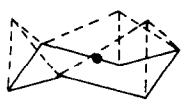

$[Au_{10}Cl_3(PCy_2Ph)_6]^+$

The computed energies of the molecular orbitals on these clusters are illustrated in Fig. 4. It can be seen that the stabilisation of the totally symmetric S^{σ} molecular orbital increases as the nuclearity increases. The P_x^{σ} and P_y^{σ} molecular orbitals are similarly stabilised, P_y^{σ} more so than P_x^{σ} leading to a degenerate HOMO in $[Au_{10}(PH_3)_9]^{4+}$. At a higher energy the P_z^{σ} orbital remains non-bonding though it is

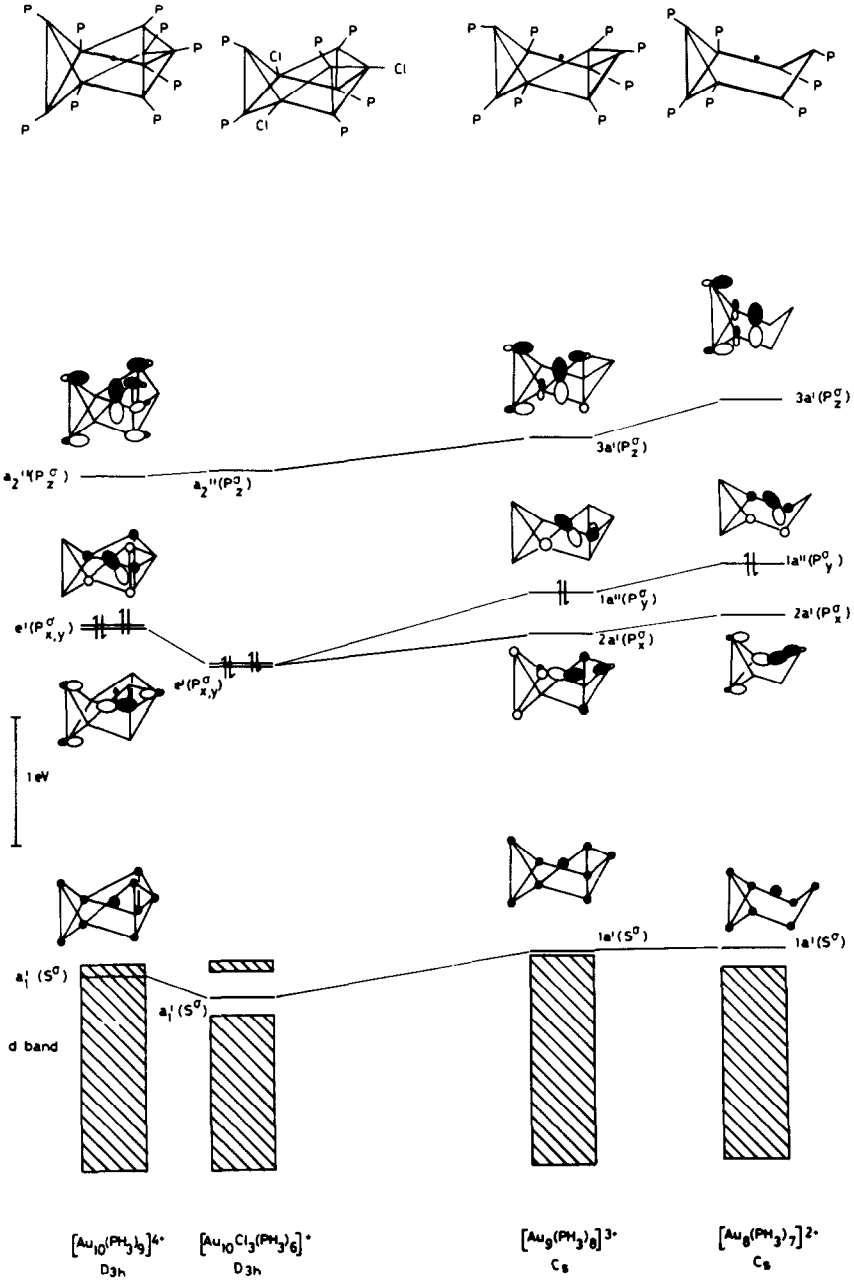

Fig. 4. The skeletal molecular orbitals for Au_8, Au_9 and Au_{10} toroidal clusters.

TABLE 4

Au–Au BOND LENGTHS IN $[Au_{10}Cl_3(PCy_2Ph)_6][NO_3]$ AND COMPUTED OVERLAP POPULATIONS FOR $[Au_{10}(PH_3)_9]^{4+}$

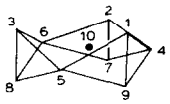

Bond	Bond lengths (Å)	Computed overlap population
10–4	2.674(1)	
10–5	2.669(1)	0.21
10–6	2.666(1)	
10–1	2.712(2)	
10–2	2.740(2)	
10–3	2.733(2)	0.19
10–7	2.703(2)	
10–8	2.728(2)	
10–9	2.729(2)	
1–9	2.738(2)	
3–8	2.744(2)	0.13
2–7	2.748(2)	
all others	2.814(2)–2.941(2)	0.10

also stabilised on increasing the nuclearity of the cluster. A calculation was also performed on $[Au_{10}Cl_3(PH_3)_6]^+$ having the same gold skeletal geometry described above but with three PH_3 units, attached to Au(4), Au(5) and Au(6), replaced by chlorine atoms. This gave a similar spectrum of energy levels with the S^σ and P_x^σ, P_y^σ molecular orbitals stabilised by 0.3 eV, as illustrated in Fig. 4.

The gold–gold bond lengths found from an X-ray crystallographic study of $[Au_{10}Cl_3(PCy_2Ph)_6][NO_3]$ are accounted for nicely in the computed overlap populations and are summarised in Table 4 [8]. Common to other gold cluster compounds the radial bonds are consistently shorter and have larger overlap populations than the peripheral bonds. Interestingly the peripheral bonds Au(1)–Au(9), Au(2)–Au(7) and Au(3)–Au(8) are shorter than the other peripheral bonds. This can be rationalised by reference to the illustrations of the e' (P_x^σ and P_y^σ) orbitals which show that the hybrid orbitals of the peripheral $Au(PH_3)$ fragments are bonding across these edges.

Detailed analysis of spherical clusters

Starting from the $Au_7(PH_3)_6$ centred chair structure alternative structures can be generated by introducing $AuPH_3$ or $Au_3(PH_3)_3$ fragments along the symmetry axis. The resultant clusters have topologies related to a sphere. For example $[Au_8(PH_3)_7]^+$ can be generated by adding an $[Au(PH_3)]^+$ fragment along the three fold axis as

shown below:

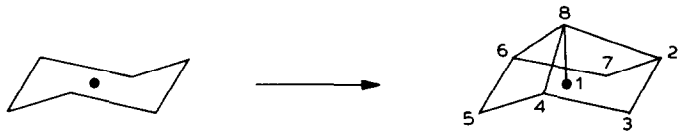

The coordination of an $AuPH_3$ unit has the effect of stabilising $1a_1(S^\sigma)$ by 0.4 eV while having little or no effect on the degenerate $e(P_x^\sigma, P_y^\sigma)$ molecular orbitals, as illustrated in Fig. 5. However, there is a dramatic stabilisation of the antibonding $2a_1(P_z^\sigma)$ orbital which now becomes the LUMO. This orbital consists essentially of an in-phase overlap of a p_z orbital on the central gold atom and an sp_z hybrid on the capping cold Au(8), as illustrated below:

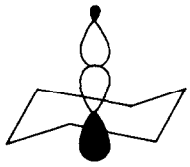

Clearly this orbital can also interact strongly with an $Au(PH_3)$ fragment or a PH_3 ligand which approaches the cluster from the opposite side. If a PH_3 ligand is brought up in this fashion then the species $[Au_8(PH_3)_8]^{2+}$ is generated. To reflect more accurately the observed structure for $[Au_8(PPh_3)_8]^{2+}$, the cyclohexane chair of gold atoms is compressed to give a more puckered ring. A calculation performed on this geometry showed that there is little change in the energies of the degenerate $e(P_x^\sigma, P_y^\sigma)$ orbitals with respect to $[Au_8(PH_3)_7]^{2+}$, but the $1a_1(S^\sigma)$ orbital is significantly destabilised on PH_3 coordination. This arises from a three orbital interaction between a low lying phosphine sp_z hybrid orbital and the $[Au_8(PH_3)_7]$ fragment $1a_1(S^\sigma)$ and $2a_1(P_z^\sigma)$ molecular orbitals as shown in Fig. 6.

The computed overlap populations reflect the observed bond lengths reasonably well, see Table 5. The bonding of the capping gold Au(8) can be thought of as almost exclusively bonded to the central gold atom, showing little interaction with other peripheral gold atoms. This is reflected in the observed very short Au(1)–Au(8) bond, and is rationalised by the PH_3 group causing a rehybridisation of the orbitals on the central gold atom giving an orbital directed at the capping gold atom.

The calculated overlap population for the Au–P bond to the central atom of 0.38 is smaller than that for the remaining Au–P bonds. Structurally this manifests itself in the very long $Au_{central}$–P bond, 2.42(1) Å compared to those normally observed (2.29 Å) [14]. Steric factors could also contribute to the length of this bond. Chemically the weakness of this bond is shown by the ability of a phosphine extractor to remove this phosphine according to the following equation [14]:

$$[Au_8(PPh_3)_8]^{2+} + 0.25[RhCl(C_8H_{14})_2]_2 \rightarrow$$

$$[Au_8(PPh_3)_7]^{2+} + 0.25[RhCl(PPh_3)_2]_2 + C_8H_{14}$$

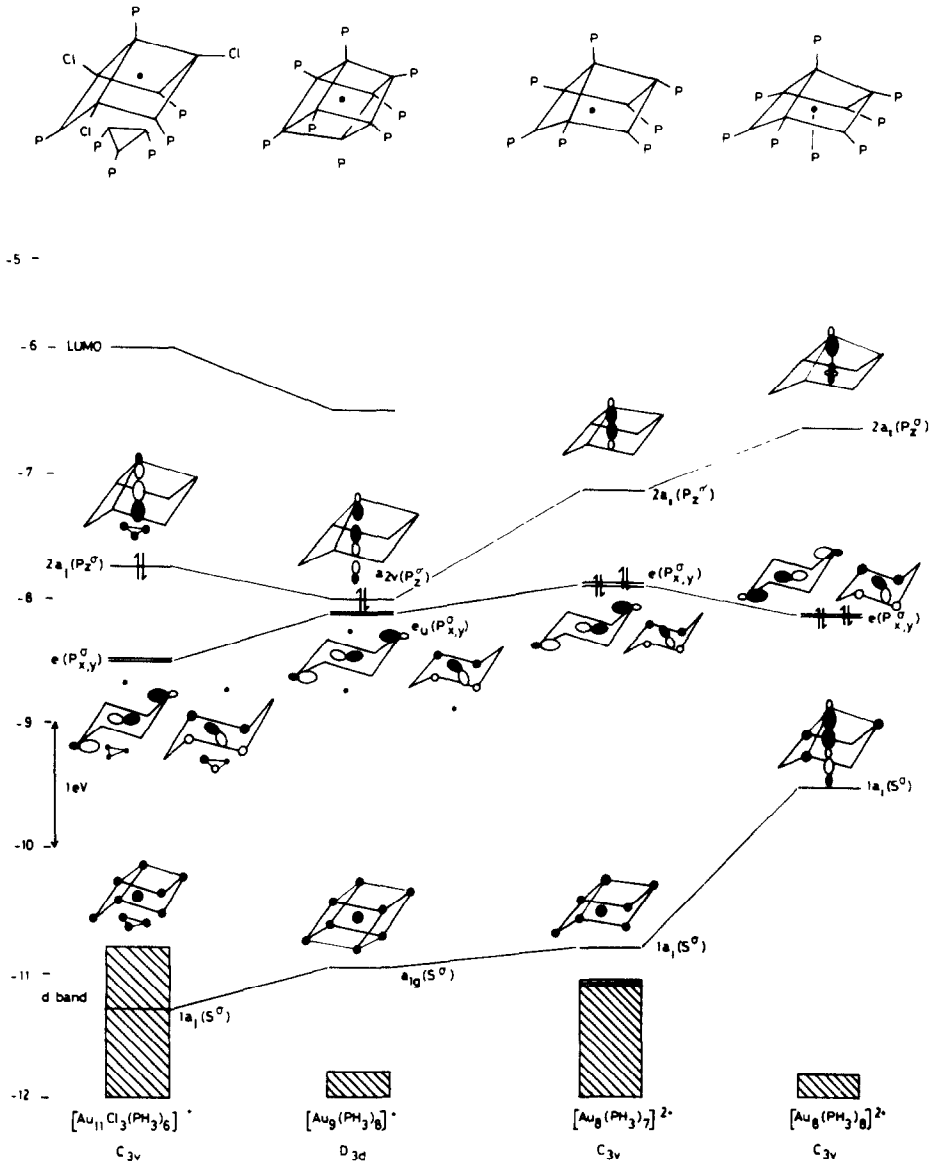

Fig. 5. The skeletal molecular orbitals for gold cluster cations with spherical topologies.

If instead of PH_3, an $AuPH_3$ fragment is brought up to an $[Au_8(PH_3)_7]$ (compressed) structure then the species $[Au_9(PH_3)_8]$ is formed, as illustrated below:

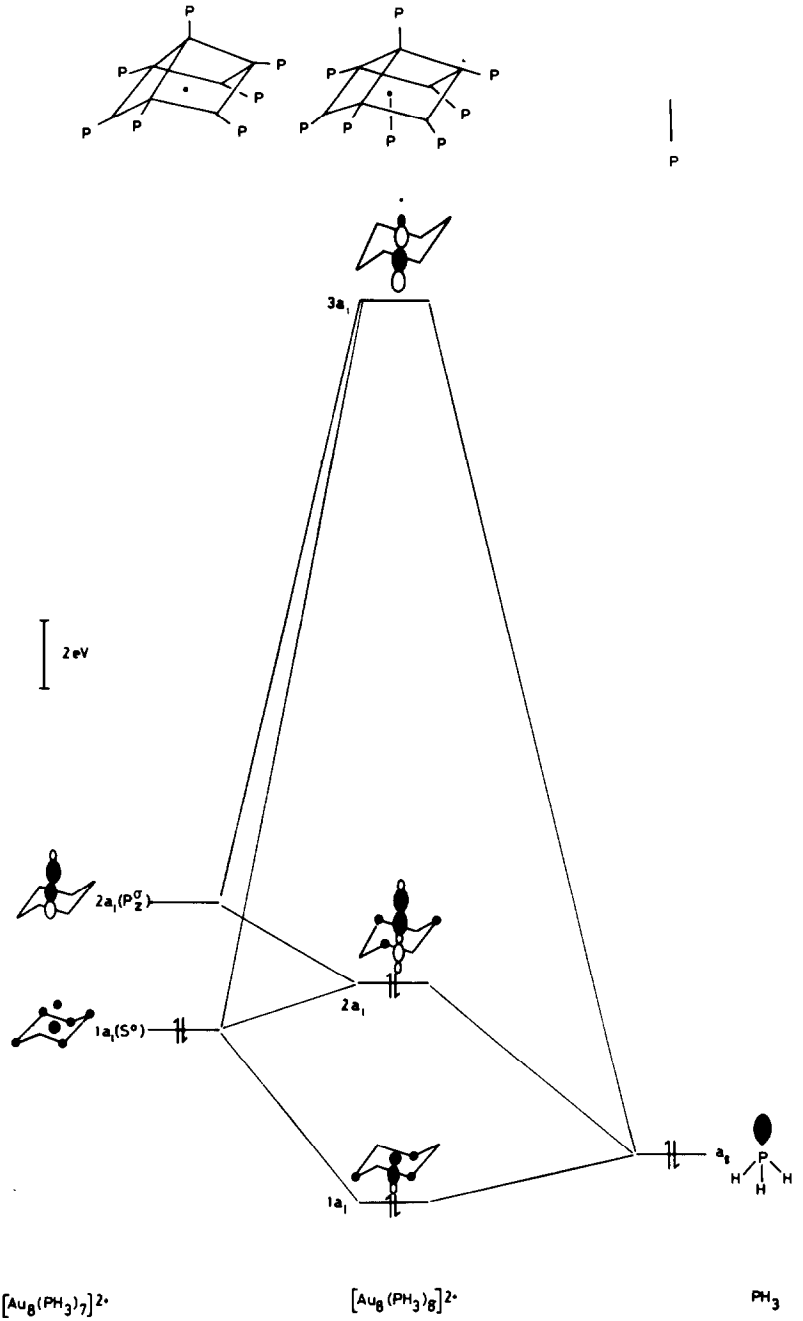

Fig. 6. The interaction diagram for the addition of a phosphine in an axial position to $[Au_8(PH_3)_7]^{2+}$, which illustrates the three-centre nature of the interaction.

Calculations performed on this molecule showed that the $a_{1g}(S^{\sigma})$ and degenerate $e_u(P_x^{\sigma}, P_y^{\sigma})$ orbitals are stabilised slightly. More interestingly however, the $a_{2u}(P_z^{\sigma})$ orbital is now brought into the bonding region by an in-phase overlap with an sp_z

TABLE 5

Au–Au BOND LENGTHS FOUND IN $[Au_8(PPh_3)_8][PF_6]_2$ AND COMPUTED OVERLAP POPULATIONS FOR $[Au_8(PH_3)_8]^{2+}$

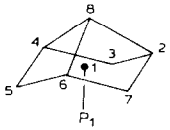

Bond	Bond lengths (Å)	Computed overlap population
1–8	2.635(8)	0.24
1–2	2.682(8)	
1–4	2.721(8)	0 25
1–6	2.709(8)	
1–3	2.723(8)	
1–5	2.707(8)	0.17
1–7	2.721(8)	
2–3, 2–7, 5–4, 5–6	2.87 ± 0.01	0.09
3–4, 6–7	2.86 ± 0.01	0.09
8–2	2 960(8)	
8–4	2 909(8)	0.06
8–6	2.932(8)	

hybrid on the $AuPH_3$ fragment as illustrated in Fig. 5. A cluster of stoicheiometry $[Au_9(PH_3)_8]^+$ would be predicted to be stable with this geometry. In fact the compound $[Au_9(PPh_3)_8][PF_6]$ has been characterised by X-ray crystallographic techniques, and although the accuracy of the structural determination was low, the geometry of the cluster is similar to that described above [20].

A further stabilisation of about 0.2 eV is achieved by twisting two triangles of gold atoms, defined by Au(2), Au(4), Au(6) and Au(3), Au(5), Au(7) with respect to each other about the three-fold axis. This distortion is observed in the solid state structure.

The two apical gold atoms show only weak interactions with other peripheral gold atoms and can be considered to be bonded mainly to the central gold atom.

The computed overlap populations for the structure having D_{3d} symmetry is shown in Table 6 together with the observed bond lengths. It can be seen that there is reasonable agreement, although it should be noted that the standard deviations associated with the gold–gold bonds are large in this structure.

If an $Au_3(PH_3)_3$ triangular fragment is brought up to $[Au_8(PH_3)_7]$ structure then

TABLE 6

Au–Au BOND LENGTHS FOUND IN $[Au_9(PPh_3)_8][PF_6]$ AND COMPUTED OVERLAP POPULATIONS FOR $[Au_9(PH_3)_8]^+$

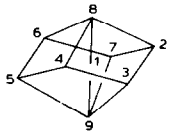

Bond	Bond lengths (Å) [a]	Computed overlap populations
1–8, 1–9	2.62	0.25
1–2, 1–7	2.55	0.25
8–2, 8–4, 8–6, 9–3, 9–5, 9–7	2.91	0.08
all others	2.7–3.4	0.08

[a] e.s.d.'s not reported but are said to be large [20].

the species $[Au_{11}(PH_3)_{10}]$ is generated as illustrated below:

The triangle $Au_3(PH_3)_3$ has an a_1 and e set of orbitals which can interact effectively with the $1a_1(S^\sigma)$, $2a_1(P_z^\sigma)$ and $e(P_x^\sigma, P_y^\sigma)$ orbitals of the $[Au_8(PH_3)_7]^{2+}$ cluster.

Extended Hückel calculations performed on $[Au_{11}(PH_3)_{10}]$ have confirmed the presence of four skeletal bonding orbitals $1a_1(S^\sigma)$, $e(P_x^\sigma, P_y^\sigma)$ and $2a_1(P_z)$, as shown in Fig. 5.

The occupation of these orbitals with 8 valence electrons would give the cluster a charge of +3. This is observed in the known undecagold cluster compounds such as $[Au_{11}(PMe_2Ph)_{10}]^{3+}$, $[Au_{11}(dppp)_5]^{3+}$, and $[Au_{11}I_3\{P(p\text{-}C_6H_4F)_3\}_7]$ [11]. Finally we note that the centred icosahedral species $[Au_{13}Cl_2(PMe_2Ph)_{10}][PF_6]_3$ also has four bonding molecular orbitals $a_g(S^\sigma)$ and $t_{1u}(P_x^\sigma, P_y^\sigma, P_z^\sigma)$. Since the bonding in this ion has been discussed in some detail previously [1] its molecular orbitals will not be analysed here.

Acknowledgements

The S.E.R.C. is thanked for its financial support.

TABLE A1

PARAMETERS FOR NON-METAL ATOMS

Atom	Orbital	Slater exponent	H_{ii} (eV)
H	1*s*	1.30	−13.60
P	3*s*	1.60	−18.60
	3*p*	1.60	−14.00
Cl	3*s*	2.03	−30.00
	3*p*	2.03	−15.00

TABLE A2

PARAMETERS FOR METAL ATOMS

Atom	Orbital	H_{ii} (eV)	ζ_1	c_1	ζ_2	c_2
Au	6*s*	−9.80	2.55			
	6*p*	−5.25	2.55			
	5*d*	−10.61	6.01	0.633	2.70	0.551

Appendix

All the calculations were performed using the extended Hückel method [18] following the procedures detailed in previous papers [1,7]. The electronic parameters which were used to input into the ICON 8 program are given in the Tables below. The phosphorus and chlorine 3*d* orbitals were omitted from the calculations after it had been established in trial calculations that they did not make a significant difference to the geometric arguments developed in the paper.

The basic centred chair of gold atoms was modelled using central to peripheral gold–gold distances of 2.87 Å and peripheral-peripheral gold–gold distances of 3.00 Å. Other structures were modelled using the same distances wherever possible. Linear $Au_{(central)}$–$Au_{(peripheral)}$–phosphorus geometries were assumed. For the PH_3 ligand P–H bond lengths of 1.42 Å and Au–P–H bond angles of 105° were used.

References

1 D.M.P. Mingos, J. Chem. Soc., Dalton Trans., (1976) 1163.
2 C.E. Briant, B.R.C. Theobald, J.W. White, L.K. Bell, A.J. Welch and D.M.P. Mingos, J. Chem. Soc., Chem. Commun., (1981) 201.
3 D.M.P. Mingos, Gold. Bulletin, 17 (1984) 5; Proc. R. Soc. Ser. A, 308 (1982) 75.
4 K.P. Hall and D.M.P. Mingos, Prog. Inorg. Chem., 32 (1984) 237.
5 J.J. Steggarda, J.J. Bour and J.W.A. van der Velden, Recl. Trav. Chim Pays, Bas., 101 (1982) 164.
6 F. De Martin, M. Manaserro, L. Naldini, R. Ruggeri and M. Sansoni, J. Chem. Commun., (1981) 22.
7 D.G. Evans and D.M.P. Mingos, J. Organomet. Chem., 232 (1982) 171.
8 C.E. Briant, K.P. Hall, A.C. Wheeler and D.M.P. Mingos, J. Chem. Soc., Chem. Commun., (1984) 248.
9 K.P. Hall, B.R.C. Theobald, D.I. Gilmour, D.M.P. Mingos and A.J. Welch, J. Chem. Soc., Chem. Commun., (1982) 528.
10 P.L. Bellon, M. Manaserro and M. Sansoni, J. Chem. Soc., Dalton Trans., (1972) 1481.

11 M. Manaserro, L. Naldini and M. Sansoni, J. Chem. Soc., Chem. Commun., (1979) 385; F.A. Vollenbroek, W.P. Bosman, J.J. Bour, J.H. Noordik and P.T. Beurskens, J. Chem. Soc., Chem. Commun., (1979) 387.
12 P.L. Bellon, F. Cariati, M. Manaserro, L. Naldini and M. Sansoni, J. Chem. Soc., Chem. Commun., (1971) 1423; J.M.M. Smits, J.J. Bour, F.A. Vollenbroek and P.T. Beurskens, J. Cryst. Spectrosc. Res., 13 (1983) 365.
13 M.K. Cooper, G.R. Dennis, K. Henrick and M. Mc Partlin, Inorg. Chim. Acta, 45 (1980) L151.
14 J.W.A. van der Velden, J.J. Bour, W.P. Bosman and J.J. Noordik, J. Chem. Soc., Chem. Commun., (1981) 1218.
15 C.E. Briant, K.P. Hall and D.M.P. Mingos, J. Chem. Soc., Chem. Commun., (1984) 290.
16 A.J. Stone, Mol. Phys., 41 (1980) 1339.
17 A.J. Stone, Inorg. Chem., 20 (1981) 503.
18 R. Hoffmann and W.N. Lipscomb, J. Chem. Phys., 36 (1982) 2179.
19 K. Wade, Adv. Inorg. Radiochem., 18 (1976) 1.
20 J.G.M. Van der Linden, M.L.H. Paulissen and J.E.J. Schmitz, J. Amer. Chem. Soc., 105 (1983) 1903.